Applied Catalysis B: Environmental 338 (2023) 123094

Contents lists available at ScienceDirect

Applied Catalysis B: Environmental

journal homepage: www.elsevier.com/locate/apcatb

Saturated Ti-coordinated {001} facets-dependent photocatalytic water reduction over NH_2-MIL-125(Ti) sheets: Observation and unraveling of facets effect

Lifang Liu [a,b,1], Shiwen Du [a,1], Yejun Xiao [c,1], Xiangyang Guo [a], Shengye Jin [c], Guosheng Shao [d], Fuxiang Zhang [a,*]

[a] State Key Laboratory of Catalysis, Dalian Institute of Chemical Physics, The Collaborative Innovation Centre of Chemistry for Energy Materials (iChEM), Dalian National Laboratory for Clean Energy, Chinese Academy of Sciences, Zhongshan Road 457, Dalian 116023, China
[b] Center of Materials Science and Optoelectronics Engineering, University of Chinese Academy of Sciences, Beijing 100049, China
[c] State Key Laboratory of Molecular Reaction Dynamics and Dynamics Research Center for Energy and Environmental Materials, Dalian Institute of Chemical Physics, Chinese Academy of Sciences, Zhongshan Road 457, Dalian 116023, China
[d] State Center for International Cooperation on Designer Low-Carbon and Environmental Materials (CDLCEM) School of Materials Science and Engineering Zhengzhou University, Zhengzhou 450001, China

ARTICLE INFO

Keywords:
Metal–organic frameworks
Photocatalyst
Water splitting
Charge separation
Hydrogen

ABSTRACT

Facets-dependent photocatalytic H_2 evolution rates of inorganic semiconductors have been well recognized, but it remains unclear for metal-organic frameworks (MOFs). Herein, we controllably prepared a series of NH_2-MIL-125(Ti) MOF sheets with different ratios of {001}/{111} facets exposure, on which the photocatalytic H_2 evolution rates from water are demonstrated to be almost linearly increased with enhanced proportion of {001} facets. Notably, the optimized activity of ca. 2640 μmol h^{-1} g^{-1} is by far superior to all the NH_2-MIL-125(Ti)-based photocatalysts reported. The discovery of facets-dependent photocatalytic water splitting performance (i.e. facets effect) was unravelled to mainly result from their distinct charge separation abilities according to the experimental facts that the saturated six-coordinated Ti atoms (Ti_{6c}) in the {001} facets can more efficiently accept and store the photogenerated electrons by the reduction of Ti^{4+} into Ti^{3+} with respect to the low-coordinated Ti atoms (Ti_{4c} and Ti_{5c}) in the {111} facets.

1. Introduction

Controllable synthesis of exposed facets and facets-dependent activity correlation over catalyst has inspired extensive interest due to its effectiveness in adjusting active site structure as well as various heterogeneous catalytic performances [1–7]. As far as photocatalysis is concerned, the charge separation and surface catalysis over many inorganic semiconductors have been demonstrated to be greatly dominated by exposed surfaces of the photocatalysts, and facet engineering has become one of the most effective strategies promoting photocatalytic performance [4,7]. For example, the facets of TiO_2, $BiVO_4$, and Ag_3PO_4 have been controllably synthesized to get insight into their facet-dependent photocatalytic activities containing reduction or oxidation functionality [4,5,8–10], and spatial charge separation has been revealed to happen among anisotropic facets of $BiVO_4$, TiO_2, BiOCl, and $SrTiO_3$, etc under the light irradiation [8,11–13]. Compared with the well-recognized facet-controlled fabrication and facets-dependent activity discussion on the inorganic semiconductor photocatalysts, however, facet engineering and its influence on the photocatalytic activity are rarely investigated and still in infancy for the metal-organic frameworks (MOFs) photocatalysts that have been advantages such as high surface area, tunable porosity, and tailorable structure, etc [14–19].

NH_2-MIL-125(Ti) is one of the most popular MOFs-type photocatalysts due to its broad visible light absorption, high stability, and unique photocatalytic properties [14,20,21]. To date, great efforts have been made to broaden its applications in the field of such as oxidation of organic compounds [22,23], photocatalytic CO_2 reduction [21,24],

* Corresponding author.
E-mail address: fxzhang@dicp.ac.cn (F. Zhang).
[1] These authors contributed equally to this work

https://doi.org/10.1016/j.apcatb.2023.123094
Received 3 April 2023; Received in revised form 4 July 2023; Accepted 9 July 2023
Available online 11 July 2023

water splitting to produce hydrogen [25,26], and photocatalytic sensors [27,28], but the development of target NH_2-MIL-125(Ti) photocatalyst with controllable reactive facets exposed and studies regarding its facet effect on the photocatalytic process are limited due to the big challenges originating from both experimental synthesis and theoretical simulation [29,30]. For example, the controllable synthesis of reactive facets exposed MOFs sheet has to confront rapid disappearance during the growth process, easy restack of individual nanosheets caused by their strong interlayer interactions, the morphological change and low yield using 3D bulk structure disintegration methods [31–34]. And theoretical simulation on the surface morphology effect of MOFs is full of great challenges because of its complicated structures, multiple chemical bonds and huge number of atoms in the theoretical computational models [35,36]. Very recently, Sun et al. have made a relatively detailed investigation on the facet effect of NH_2-MIL-125(Ti) photocatalyst on the CO_2 reduction performance from the viewpoint of both high-index and low-index facets [37,38], demonstrating that the exposed high-index facets such as {112} facets are more favorable for the CO_2 reduction with respect to the low-index {001} and {111} facets. However, the activity dependence of water splitting on the NH_2-MIL-125(Ti) with low-index facets exposed and underlying understanding has been rarely discussed.

Herein, we controllably synthesized a series of NH_2-MIL-125(Ti) MOF sheets with different ratios of {001}/{111} facets by a conventional hydrothermal method under the assistance of different amounts of morphology control agent (monocarboxylic thioglycolic acid, MTA), on which the facet-dependent water reduction rates under visible light irradiation were investigated in detail. The MTA could be preferentially adsorbed on the {001} facets to regulate its growth kinetics, and excessive acid will act as a competitor to compete with 2-aminoterephthalic acid (H_2ATA) ligand and inhibit the growth of nuclei, leading to the formation of thick crystals. As for convenient discussion, the corresponding samples are denoted as MIL(Ti)-n, where n stands for the percentage of exposed {001} facets. Under the modification of platinum cocatalyst, the hydrogen evolution rates on the Pt/MIL(Ti)-n are found to be almost linearly enhanced with increasing ratio of exposed {001} facets, demonstrating existence of the facets effect.

2. Experimental section

2.1. Synthesis of MIL(Ti)-n sheets and Pt/MIL(Ti)-n

H_2ATA (163 mg) was dissolved in 3 mL of the mixture between EtOH and DMF (1:1 (v/v)) under stirring for 20 min. After adding thioglycolic acid ($C_2H_4O_2S$, 300 μL, 325 μL, 350 μL, 375 μL, 400 μL) and $Ti(C_3H_7O)_4$ (90 μL), stirring for 20 min, then moved the liquid in a 20 mL reactor, sealed in a constant temperature oven at 150 °C for 15 h. Finally, the yellow precipitates were formed after being cooled to room temperature and then collected by centrifugation, washed by DMF and EtOH for three times, and dried in a vacuum oven overnight.

H_2PtCl_6 aqueous solution (400 μL, 1 mg mL^{-1},) was added into 20 mg MIL(Ti)-n sheets powder, and then dried at 80 °C under stirring. The platinum-modified MIL(Ti)-n (Pt/MIL(Ti)-n, 2 wt% Pt) were reduced with 5% H_2/Ar at 473 K for 2 h.

2.2. Photoelectrochemical measurements

All the photoelectrochemical measurements were conducted on Solartron Analytical workstation with a standard three-electrode system. MIL(Ti)-n-coated FTO as the working electrode, platinum sheet as the counter electrode, and Ag/AgCl as the reference electrode. The electrolyte was 0.1 M Na_2SO_4 aqueous solution. The electrochemical impedance spectroscopy (EIS) was measured at 0.6 V vs. RHE under AM 1.5 G illumination. Liner sweep voltage (LSV) measurements were measured in the voltage window of 0.4–1.2 V vs. RHE under AM 1.5 G illumination.

2.3. Photocatalytic reactions for hydrogen evolution

Pt/MIL(Ti)-n samples (20 mg) were added into a reaction vessel with Pyrex top-irradiation type, and the reaction vessel was connected to an evacuation device containing a mixture of CH_3CN (83 mL), deionized water (2 mL), and TEOA (15 mL, hole sacrificial agent). After that, the reaction vessel and reaction suspension were degassed completely using a vacuum pump. Finally, the reaction suspension was photo-irradiated by a 300 W xenon lamp with work current of 15 mA, an 420 nm optical filter was used to cutoff the ultraviolet light and installed on the xenon lamp, and the cooling water was used to keep the reaction suspension at 15 °C by a circular cooling water device. The gas products

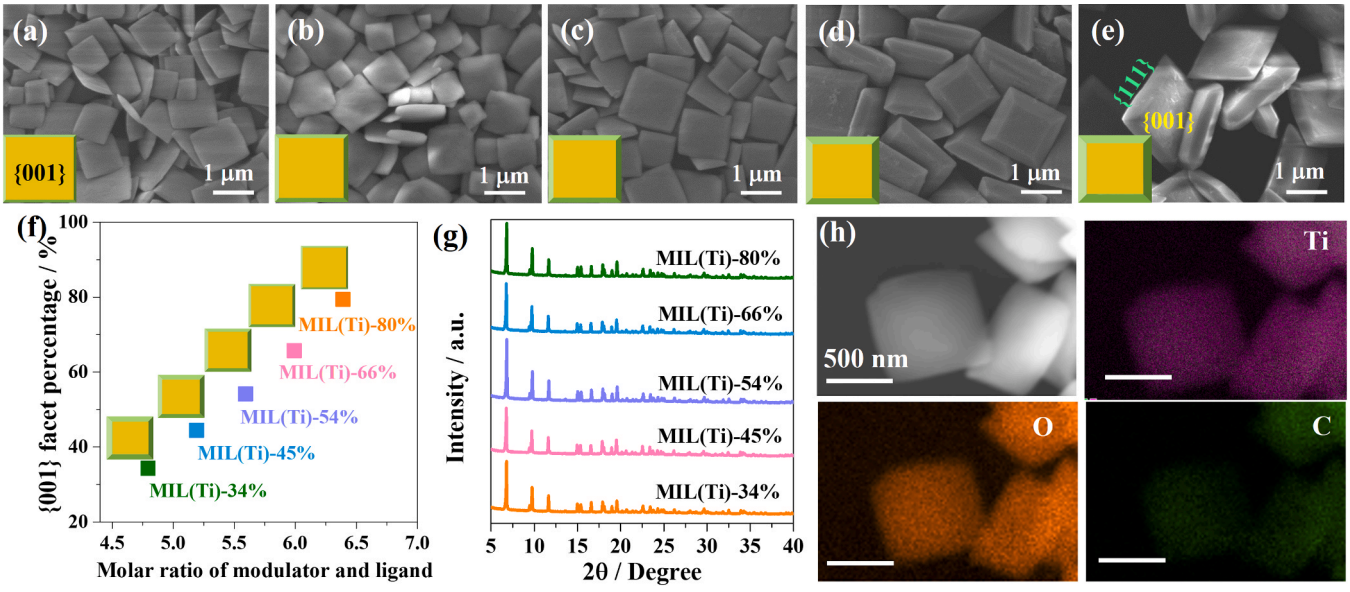

Fig. 1. (a)-(e) SEM images of MIL(Ti)-n (Inset: the geometric models), (f) {001} facets exposed ratios, and (g) XRD patterns of MIL(Ti)-n. (h) SEM-EDS elemental mapping of MIL(Ti)– 80% sheets.

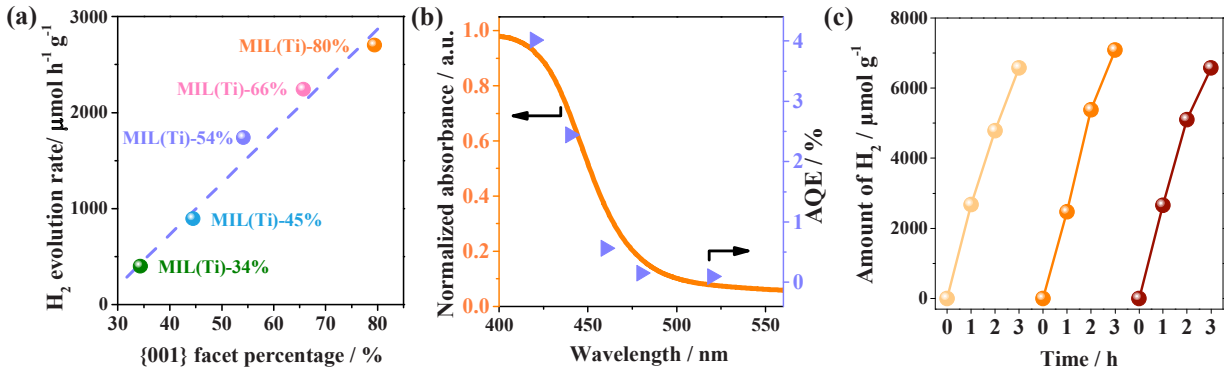

Fig. 2. (a) The relative diagram of H_2 evolution rate and facet percentages of {001} facets of Pt/MIL(Ti)-n. (b) The apparent quantum efficiencies of photocatalytic H_2 evolution reaction and absorption spectrum of Pt/MIL(Ti)− 80% sheets. (c) The circular experiment of photocatalytic H_2 evolution on Pt/MIL(Ti)− 80% sheets.

were analyzed by Shimadzu GC-2014 gas chromatography. Recycling experiments were conducted by adding the consumed reaction solution and keeping vacuum again.

2.4. Catalysts characterizations and computational details

Full details of the FI-IR spectra, XRD patterns, SEM images, charge separation efficiency calculations, AQE calculations, XPS, EPR, PL, TRPL, TA kinetics measurements, and computational calculations are described in the Supporting Information.

3. Results and discussion

3.1. Morphology and structure of MIL(Ti)-n samples

Fig. 1 gives the typical morphologies of series MIL(Ti)-n prepared, in which all the MIL(Ti)–n crystals exhibit similar morphology of decahedral sheets (Fig. 1a-e) but with different ratios exposure of low-index {001} and {111} facets (Fig. 1f and Table S1). Similar X-ray diffraction (XRD) peaks (Fig. 1g) and characteristic peaks of Fourier-transform infrared (FT-IR) spectra (Fig. S1) are observed for all of them, demonstrating their similar crystallinity and local structures. As one of the most typical features in the MOFs materials, the homogeneous distribution of Ti, O, and C elements is similarly observed in this work according to the energy dispersive spectra (EDS) analysis (Fig. 1h).

3.2. Activity tests of the Pt/MIL(Ti)-n samples

The facets effect on the photocatalytic water reduction activity was explored by employing the Pt/MIL(Ti)-n sheets as photocatalysts in the presence of triethanolamine (TEOA, as hole sacrificial agent) under visible-light irradiation ($\lambda \geq 420$ nm). As shown in Fig. 2a, the photocatalytic H_2 production rates are closely related to the ratio of exposed {001}/{111} facets, which are almost linearly increased with the enhanced percentages of exposed {001} facets. This means that the remarkable facets effect happens on the MIL(Ti)-n photocatalysts, and the {001} facets are more favorable for the water reduction with respect to the {111} facets. Meanwhile, the Pt/MIL(Ti)− 80% sheets exhibit the highest H_2 evolution rate of 2640 μmol h^{-1} g^{-1} (i.e. 53 μmol h^{-1}), which is about 8 times higher than that of Pt/MIL(Ti)− 34% sheets (318 μmol h^{-1} g^{-1}). It is worth noting that the H_2 evolution rate on the Pt/MIL(Ti)− 80% sheets is also superior to other NH_2-MIL-125(Ti) photocatalysts reported (Table S2). The apparent quantum efficiencies (AQEs) of H_2 evolution over the Pt/MIL(Ti)− 80% sheets were measured under different monochromic light irradiation, which are in good agreement with its light absorption coefficient (Fig. 2b), revealing that its activities result from the photocatalytic process. The obtained maximal AQE is 4.0% at 420 ± 10 nm. The as-synthesized MIL(Ti)− 80% sheets are of good photochemical stability based on the multiple cycles of results (Fig. 2c) and unobvious change of SEM images, XRD patterns, FT–IR spectra and XPS results after the photocatalytic reaction (Figs. S2–5).

3.3. Underlying understanding of facets effect

To unravel the facets effect on the photocatalytic water splitting to produce hydrogen, the basic processes of photocatalysis involving light absorption, charge separation, and surface reaction on the series of MIL (Ti)-n samples were thus compared and analyzed. As seen in the UV–vis diffuse reflectance spectra (Fig. 3a), all the samples exhibit good visible light absorption edges with continuously blue-shifted as the increasing ratio of {001}/{111} facets. This means that the increased exposure of {001} facets is unfavorable for light absorption, leading to decreased

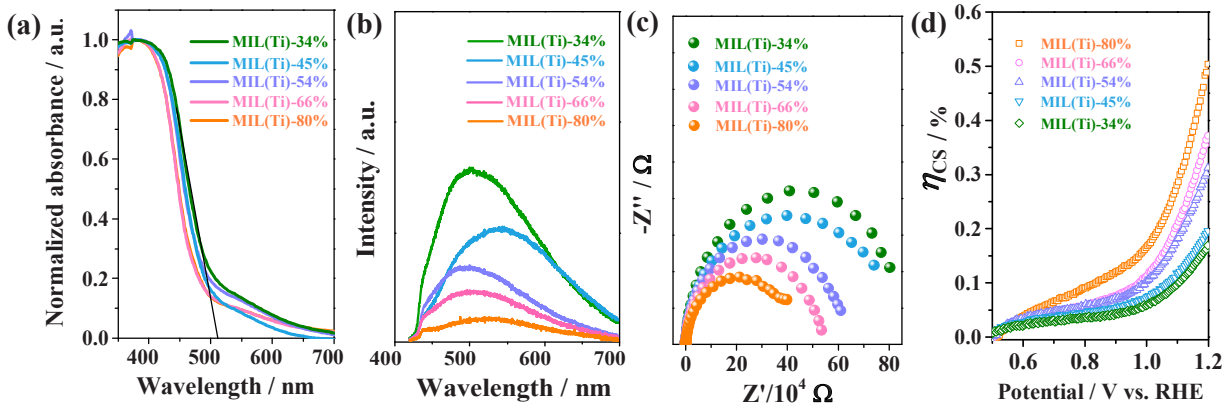

Fig. 3. (a) UV–vis diffuse reflectance spectra, (b) Steady-state photoluminescence (PL) spectra, (c) EIS, and (d) Charge separation efficiency (η_{CS}) of MIL(Ti)-n sheets.

light absorption efficiency. In this case, the trend of light absorption on them is almost opposite to the activity trend observed in Fig. 2a, so it is reasonable to deduce that the light absorption should not be the main factor causing their distinct water splitting activities. Additionally, the exposed surface areas of them are similar according to their N_2 adsorption isotherms (Fig. S6), and the amounts of platinum cocatalysts on the MIL(Ti)-n samples are similar as well. Accordingly, we can reasonably expect that the efficiencies of surface catalysis on them are closely consistent.

It has been widely known that the efficiency/activity of one photocatalyst for water splitting is synergistically determined by light absorption (η_{LA}), charge separation (η_{CS}), and surface catalysis (η_{SC}) (i.e. η % = $\eta_{LA} \times \eta_{CS} \times \eta_{SC}$) [39,40]. In this work, as above mentioned, the order of light absorption efficiencies is opposite to that of activity, and the efficiencies of surface catalysis are similar. Therefore, the facets-dependent photocatalytic water splitting activities are proposed to be predominantly determined by their charge separation efficiencies. In order to verify our speculation, the steady-state photoluminescence (PL) spectra on them were firstly examined with results given in Fig. 3b, where the intensities of PL peaks near their band edges are continuously decreased with increasing ratio of {001}/{111} facets. This well reveals that the sample with increased exposure of {001} facets could remarkably suppress the photogenerated electron-hole recombination, leading to increased charge separation efficiency. Secondly, according to the results of their charge transfer resistances detected by the electrochemical impedance spectra (EIS) (Fig. 3c), the same charge separation order as the PL analysis can be deduced. Thirdly, their charge separation efficiencies were calculated by the photoelectrochemical performances measured in the electrolyte with Na_2SO_3 hole scavenger [41]. As given in Fig. 3d and Fig. S7, the similar trend of charge separation can be further observed. The above analysis and discussion results consistently support that their different properties of charge separation are the main factor in determining the facets-dependent photocatalytic performances.

3.4. Unraveling of facets effect on the charge separation

In order to understand the underlying influencing mechanism of the distinct facets exposed on their charge eparation, both theoretical calculation and structural characterizations on the typical samples MIL(Ti)− 34% and MIL(Ti)− 80% with separately minimal and maximal percentage of exposed {001} facets were carried out. First of all, the density functional theory (DFT) calculations were carried out to get insight of the local coordination environments of {001} and {111} facets, which were constructed by following the principle of consuming minimal energy to create surface slabs for MOFs [35]. As seen in Fig. 4a and 4b, the {001} facets are mainly composed of saturated six-coordinated Ti atoms (Ti_{6c}), while the {111} facets are composed of both Ti_{6c} and low-coordinated Ti atoms (Ti_{4c} and Ti_{5c}). Moreover, much more abundant Ti-O clusters should exist on the {001} facets with respect to the {111} facets, as is well further confirmed by the results of energy-dispersive spectra (EDS) (Fig. S8), where a higher percentage of Ti atoms is observed for the {001} facets. This is consistent with the comparison of crystal inherent structure along the {001} and {111} directions (Fig. S9). The more abundant Ti^{4+} ions on the {001} facets can be further confirmed by the results of Ti 2p X-ray photoelectron spectroscopy (XPS) analysis (Fig. 4c), where the Ti 2p binding energy in the MIL(Ti)− 80% sheets is 0.2 eV positively shifted with respect to the MIL(Ti)− 34% sample.

Secondly, the *in-situ* EPR measurement was carried out to compare the local structural change of MIL(Ti)− 80% and MIL(Ti)− 34% samples under the light irradiation and dark conditions, in consideration that the

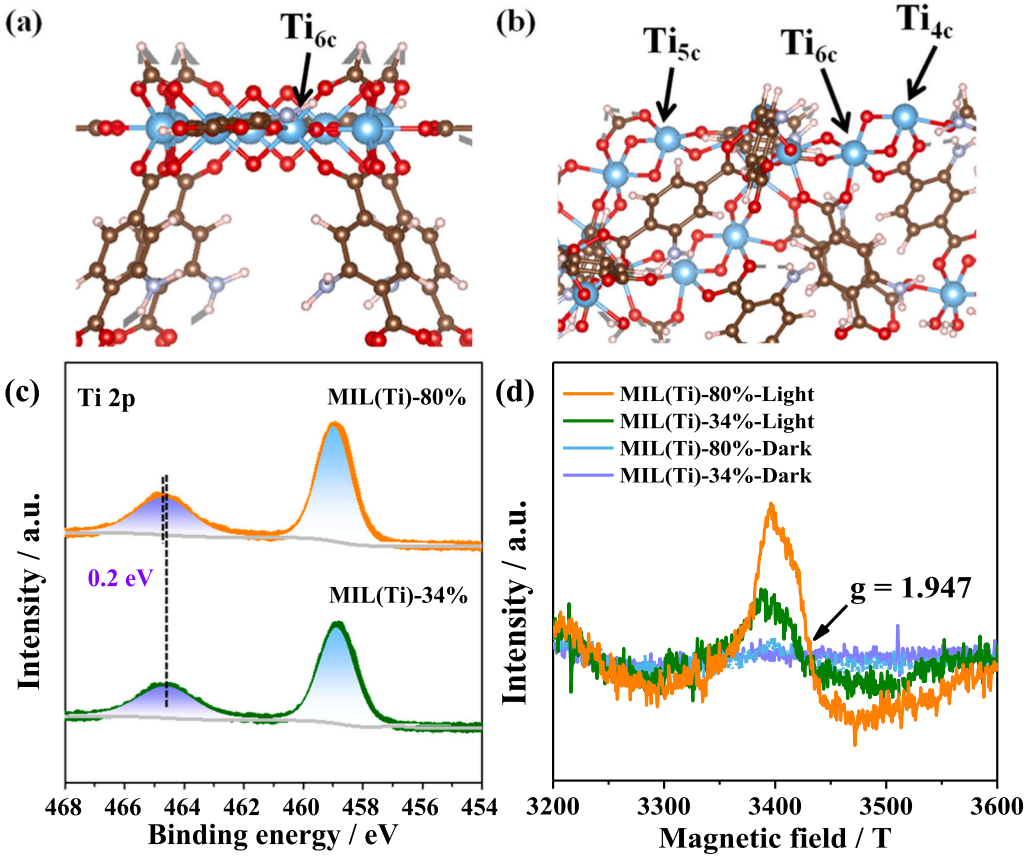

Fig. 4. (a) and (b) {001} and {111} surface exposed atoms in the MIL(Ti)-(n). (c) XPS of Ti element of MIL(Ti)− 80%, and MIL(Ti)− 34%. (d) EPR spectra of MIL(Ti)− 80%, and MIL(Ti)− 34% under dark and light condition.

ligand to metal node charge transfer (LMCT) has been demonstrated to occur in the NH_2-MIL-125(Ti) photocatalysts to cause probable reduction of Ti^{4+} into Ti^{3+} ions during the light irradiation [21,42]. As given in Fig. 4d, the signal peak located at g value of 1.947 assigned to the formed Ti^{3+} species is clearly observed for both samples, in accordance with previous results. It is worth noting that the intensities of Ti^{3+} peak are closely related to the ratio of exposed {001}/{111} facets, which is much larger on the MIL(Ti)− 80% sample with respect to the MIL(Ti)− 34%. This means that much more amount of Ti^{3+} species are formed on the MIL(Ti)− 80% sample under the light irradiation, as is in good accordance with the fact that much higher content of saturated six-coordinated Ti^{4+} ions exist in the MIL(Ti)− 80% sample with higher content of {001} facets (Fig. 4a-c). On this basis, it is reasonable to deduce that the saturated six-coordinated Ti^{4+} ions tend to better accept the photogenerated electrons from the ligand and store them into Ti ions via the reduction of Ti^{4+} into Ti^{3+} process compared with the low-coordinated Ti atoms, as should be well responsible for the superior ability of the {001} facets in promoting charge separation as well as photocatalytic activity.

Thirdly, femtosecond transient absorption (TA) spectroscopy and time-resolved photoluminescence (TRPL) spectra measurements on the typical samples were carried out to directly investigate the influence of facets effect on the charge separation. As given in Fig. S10, the TA spectra of MIL(Ti)− 34% and MIL(Ti)− 80% samples exhibit similar negative bleach peaks at 450 nm respectively, which can be attributed to the ground state bleach (GSB) according to their UV–vis absorption, demonstrating that the different facets do not significantly affect the absorption edge (Fig. 3a). Based on the fitting results of TA kinetics traces by biexponential function (Fig. 5a and Table S3), the MIL(Ti)− 80% exhibits remarkably prolonged lifetime of carriers compared to the MIL(Ti)− 34%, revealing that the enhanced exposure of {001} facets with abundant saturated six-coordinated Ti sites makes a better promotion on the separation efficiency of photogenerated carriers. A similar conclusion can be obtained according to the results of the TRPL kinetics (Fig. 5b and Table S4), where the MIL(Ti)− 80% decays faster with respect to MIL(Ti)− 34% and exhibits more efficient suppression of electron-hole recombination. Moreover, the modification of platinum cocatalysts could further promote the charge transfer with respect to their corresponding pristine partners (Fig. S11), accompanying with faster GSB kinetics decline and decreased lifetime (Table S3). This indicates that the Pt cocatalysts could effectively extract the electrons from the Ti atoms to favor the charge separation, as was also confirmed by the in-situ EPR experimental results (Fig. 5c), where the observed Ti^{3+} species signal peak located at 1.947 under light irradiation are disappeared after loading of Pt cocatalysts.

According to the above analysis, we can make a simple schematic description of the charge transfer and separation on the Pt/MIL(Ti)-n photocatalysts (Fig. 5d) as follows: i) as benefitted by the LMCT process, the photogenerated electrons originating from the excitation of ligands will be transferred to the Ti^{4+} nodes. ii) The Ti^{4+} nodes tend to be reduced into Ti^{3+} by the photogenerated electrons to store the energy. iii) The stored electrons in the Ti^{3+} sites can be easily trapped and transferred to the loaded platinum cocatalysts with higher work function for further effective reduction of water accompanying with recovery of Ti^{3+} into Ti^{4+} ions simultaneously. Since the reduction of Ti^{4+} into Ti^{3+} to accept and store the photogenerated electrons is one of the most important steps, the facets with abundant saturated six-coordinated Ti^{4+} ions play a positive effect on the charge separation as well as photocatalytic performance. This should be well responsible for the facets effect observed in this work.

As an extended discussion on the facets effect on the charge separation, DFT calculations on the work function of the {001} and {111}

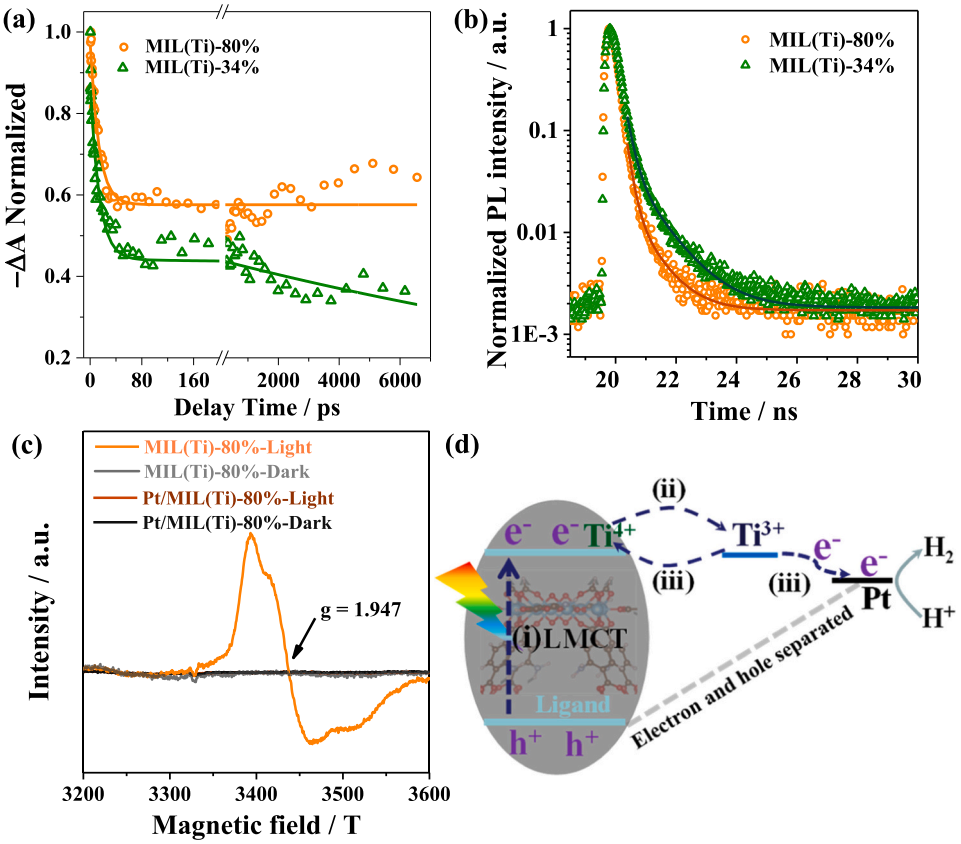

Fig. 5. (a) Comparison of normalized TA kinetics probed at indicated wavelengths (450 nm) in MIL(Ti)− 80% and MIL-(Ti)− 34% sheets. (b) Time-resolved fluorescence decay kinetics of MIL(Ti)− 80% and MIL(Ti)− 34%. (c) EPR of MIL(Ti)− 80% and Pt/MIL(Ti)− 80% sheets under light irradiation and dark. (d) Schematic diagram of photocatalytic charge transfer of Pt/MIL(Ti)-n.

facets were also carried out. As given in Fig. S12, the as-obtained work function on the {001} facets with Ti_{6c} atoms completely exposed is much higher than that on the {111} facets, rendering the {001} facets to be easier to accept photogenerated electrons. Additionally, no obvious spatial charge separation can be observed among the {001} and {111} facets of both MIL(Ti)− 80% and MIL(Ti)− 34% samples under the light irradiation, in consideration of the fact that the photo-deposited Pt or Au nanoparticles are randomly observed on both {001} and {111} facets (Fig. S13). Accordingly, the promoted charge separation observed in this work should not originate from spatial charge separation among different facets that has been recently demonstrated in many inorganic-semiconductor photocatalysts such as TiO_2 [11,43] and $BiVO_4$ [8].

4. Conclusions

We controllably synthesized a series of NH_2-MIL-125(Ti) sheets (MIL (Ti)-n (n = 34, 45, 54, 66, 80%) with different percentages of exposed {001} facets by a simple solvothermal process, based on which the facets-dependent photocatalytic water splitting performances were observed and discussed in details. Specifically, the higher content of exposed {001} facets with abundant saturated six-coordinated Ti atoms (Ti_{6c}) is, the better photocatalytic rate of hydrogen evolution from water is. The underlying working mechanism was unraveled to mainly originate from the facets effect on the charge separation, where the facets with more saturated six-coordinated Ti atoms exposed are more favorable to capture and transfer the photogenerated electrons via the LMCT process. Together with the modification of platinum cocatalyst, both charge separation and surface catalysis can be remarkably promoted, as is responsible for the benchmarking activity observed among all the reported NH_2-MIL-125(Ti)-based photocatalysts. Our results not only provide a new understanding of the facets effect from the view distinct from previous inorganic semiconductor photocatalysts, but also demonstrate the feasibility and importance of utilizing low-index facets in fabricating efficient photocatalytic systems, as may provide an alternative way of promoting solar energy conversion.

CRediT authorship contribution statement

Lifang Liu: Performing experiments, Data curation, Writing. **Shiwen Du**: Investigation, Theoretical calculation, Reviewing. **Yejun Xiao**: Performing TA experiments, Reviewing. **Xiangyang Guo**: Formal analysis, Reviewing, and Funding acquisition. **Shengye Jin**: Software, Project administration. **Guosheng Shao**: Editing, Software, Project administration. **Fuxiang Zhang**: Reviewing, Formal analysis, Conceptualization, Supervision, Visualization, Funding acquisition.

Declaration of Competing Interest

The authors declare that they have no known competing financial interests or personal relationships that could have appeared to influence the work reported in this paper.

Data Availability

Data will be made available on request.

Acknowledgments

This work was supported by the National Natural Science Foundation of China (21925206, 21901240, 22261160369), International Partnership Program of Chinese Academy of Sciences (121421KYSB20190025), Dalian Supports High-level Talent Innovation and Entrepreneurship Projects (2020RD06).

Appendix A. Supporting information

Supplementary data associated with this article can be found in the online version at doi:10.1016/j.apcatb.2023.123094.

References

[1] Y.G. Sun, Y.N. Xia, Science 298 (2002) 2176–2179.
[2] Y.J. Xiong, Y.N. Xia, Adv. Mater. 19 (2007) 3385–3391.
[3] N. Tian, Z.Y. Zhou, S.G. Sun, Y. Ding, Z.L. Wang, Science 316 (2007) 732–735.
[4] H.G. Yang, C.H. Sun, S.Z. Qiao, J. Zou, G. Liu, S.C. Smith, H.M. Cheng, G.Q. Lu, Nature 453 (2008) 638–641.
[5] Y. Bi, S. Ouyang, N. Umezawa, J. Cao, J. Ye, J. Am. Chem. Soc. 133 (2011) 6490–6492.
[6] K.B. Zhou, Y.D. Li, Angew. Chem. Int. Ed. 51 (2012) 602–613.
[7] C. Xiao, B.-A. Lu, P. Xue, N. Tian, Z.-Y. Zhou, X. Lin, W.-F. Lin, S.-G. Sun, Joule 4 (2020) 2562–2598.
[8] R.G. Li, F.X. Zhang, D.G. Wang, J.X. Yang, M.R. Li, J. Zhu, X. Zhou, H.X. Han, C. Li, Nat. Commun. 4 (2013) 1432.
[9] J. Qu, Y. Wang, X. Mu, J. Hu, B. Zeng, Y. Lu, M. Sui, R. Li, C. Li, Adv. Mater. 34 (2022) 2203320.
[10] D. Wang, H. Jiang, X. Zong, Q. Xu, Y. Ma, G. Li, C. Li, Chem. Eur. J. 17 (2011) 1275–1282.
[11] S.K. Wallace, K.P. McKenna, J. Phys. Chem. C. 119 (2015) 1913–1920.
[12] M. Li, S. Yu, H. Huang, X. Li, Y. Feng, C. Wang, Y. Wang, T. Ma, L. Guo, Y. Zhang, Angew. Chem. Int. Ed. 58 (2019) 9517–9521.
[13] L. Mu, Y. Zhao, A. Li, S. Wang, Z. Wang, J. Yang, Y. Wang, T. Liu, R. Chen, J. Zhu, F. Fan, R. Li, C. Li, Energy Environ. Sci. 9 (2016) 2463–2469.
[14] L. Li, X.-S. Wang, T.-F. Liu, J. Ye, Small Methods 4 (2020) 2000486–2000514.
[15] H.-C. Zhou, J.R. Long, O.M. Yaghi, Chem. Rev. 112 (2012) 673–674.
[16] H. Furukawa, K.E. Cordova, M. O'Keeffe, O.M. Yaghi, Science 341 (2013) 974.
[17] Y. Shi, A.-F. Yang, C.-S. Cao, B. Zhao, Coord. Chem. Rev, 390, 2019, pp. 50–75.
[18] T. Zhang, Y. Jin, Y. Shi, M. Li, J. Li, C. Duan, Coord. Chem. Rev. 380 (2019) 201–229.
[19] X. Guo, L. Liu, Y. Xiao, Y. Qi, C. Duan, F. Zhang, Coord. Chem. Rev. 435 (2021), 213785.
[20] J. Zhu, P.-Z. Li, W. Guo, Y. Zhao, R. Zou, Coord. Chem. Rev. 359 (2018) 80–101.
[21] Y. Fu, D. Sun, Y. Chen, R. Huang, Z. Ding, X. Fu, Z. Li, Angew. Chem. Int. Ed. 51 (2012) 3364–3367.
[22] X. Li, Z. Le, X. Chen, Z. Li, W. Wang, X. Liu, A. Wu, P. Xu, D. Zhang, Appl. Catal. B 236 (2018) 501–508.
[23] A. Gomez-Aviles, M. Penas-Garzon, J. Bedia, D.D. Dionysiou, J.J. Rodriguez, C. Belver, Appl. Catal. B 253 (2019) 253–262.
[24] F. Guo, M. Yang, R.-X. Li, Z.-Z. He, Y. Wang, W.-Y. Sun, ACS Catal. 12 (2022) 9486–9493.
[25] Y. Horiuchi, T. Toyao, M. Saito, K. Mochizuki, M. Iwata, H. Higashimura, M. Anpo, M. Matsuoka, J. Phys. Chem. C. 116 (2012) 20848–20853.
[26] C. Zhang, C. Xie, Y. Gao, X. Tao, C. Ding, F. Fan, H.-L. Jiang, Angew. Chem. Int. Ed. 61 (2022), e202204108.
[27] L.E. Kreno, K. Leong, O.K. Farha, M. Allendorf, R.P. Van Duyne, J.T. Hupp, Chem. Rev. 112 (2012) 1105–1125.
[28] Q. Xu, Y. Wang, G. Jin, D. Jin, K. Li, A. Mao, X. Hu, Sens. Actuators B 201 (2014) 274–280.
[29] M.J. Van Vleet, T. Weng, X. Li, J.R. Schmidt, Chem. Rev. 118 (2018) 3681–3721.
[30] F. Guo, J.-H. Guo, P. Wang, Y.-S. Kang, Y. Liu, J. Zhao, W.-Y. Sun, Chem. Sci. 10 (2019) 4834–4838.
[31] L. Kollias, R. Rousseau, V.-A. Glezakou, M. Salvalaglio, J. Am. Chem. Soc. 144 (2022) 11099–11109.
[32] M. Zhao, Y. Huang, Y. Peng, Z. Huang, Q. Ma, H. Zhang, Chem. Soc. Rev. 47 (2018) 6267–6295.
[33] R.-J. Wei, P.-Y. You, H. Duan, M. Xie, R.-Q. Xia, X. Chen, X. Zhao, G.-H. Ning, A. I. Cooper, D. Li, J. Am. Chem. Soc. (2022) 17487–17495.
[34] J.-H. Deng, Y.-Q. Wen, J. Willman, W.-J. Liu, Y.-N. Gong, D.-C. Zhong, T.-B. Lu, H.-C. Zhou, Inorg. Chem. 58 (2019) 11020–11027.
[35] S. Amirjalayer, M. Tafipolsky, R. Schmid, J. Phys. Chem. Lett. 5 (2014) 3206–3210.
[36] B. Motevalli, N. Taherifar, H. Wang, J.Z. Liu, J. Phys. Chem. C. 121 (2017) 2221–2227.
[37] X.-M. Cheng, Y. Gu, X.-Y. Zhang, X.-Y. Dao, S.-Q. Wang, J. Ma, J. Zhao, W.-Y. Sun, Appl. Catal. B 298 (2021), 120524.
[38] X.-M. Cheng, X.-Y. Zhang, X.-Y. Dao, S.-Q. Wang, J. Zhao, W.-Y. Sun, Chem. Eng. J. 431 (2022), 134125.
[39] Q. Wang, K. Domen, Chem. Rev. 120 (2020) 919–985.
[40] S. Navalón, A. Dhakshinamoorthy, M. Álvaro, B. Ferrer, H. García, Chem. Rev. 123 (2023) 445–490.
[41] T.W. Kim, K.-S. Choi, Science 343 (2014) 990–994.
[42] M. Dan-Hardi, C. Serre, T. Frot, L. Rozes, G. Maurin, C. Sanchez, G. Férey, J. Am. Chem. Soc. 131 (2009) 10857–10859.
[43] Z. Pei, S. Weng, P. Liu, Appl. Catal. B 180 (2016) 463–470.